chemosensors

Article

Fluorescent Analogues of FRH Peptide: Cu(II) Binding and Interactions with ds-DNA/RNA

Marta Košćak, Ivona Krošl, Biserka Žinić and Ivo Piantanida *

Division of Organic Chemistry and Biochemistry, Rudjer Boskovic Institute, Bijenicka Cesta 54, 10000 Zagreb, Croatia; Marta.Koscak@irb.hr (M.K.); Ivona.Krosl@irb.hr (I.K.); Biserka.Zinic@irb.hr (B.Ž.)
* Correspondence: ivo.piantanida@irb.hr; Tel.: +385-1-4571-326

Abstract: Four novel peptidoids, derived from the Phe-Arg-His (FRH) peptide motif, were prepared by replacing the histidine heterocycle with triazole and consequent triazole-fluorophore (coumarin) extension and also replacing arginine with less voluminous lysine. So the constructed Phe-Lys-Ala(triazole) (FKA(triazole)) peptidoids bind Cu^{2+} cations in water with a strong, nanomolar affinity comparable to the parent FRH and its known analogs, demonstrating that triazole can coordinate copper similarly as histidine. Moreover, even short KA(triazole)coumarin showed submicromolar affinity to Cu^{2+}. Only FKA(triazole)coumarin with free amino groups and its shorter analog KA(triazole)coumarin showed strong induced CD spectra upon Cu^{2+} cation binding. Thus, KA(triazole)coumarin can be considered as the shortest peptidoid sequence with highly sensitive fluorescent and chiral CD response for Cu^{2+} cation, encouraging further studies with other metal cations. The FKA(triazole) coumarin peptidoids show biorelevant, 10 μM affinity to ds-DNA and ds-RNA, binding within DNA/RNA grooves. Intriguingly, only peptidoid complexes with Cu^{2+} strongly stabilize ds-DNA and ds-RNA against thermal denaturation, suggesting significant interactions of Cu^{2+} cation within the DNA/RNA binding site.

Keywords: fluorescent peptide; circular dichroism; copper-binding; DNA/RNA binding

Citation: Košćak, M.; Krošl, I.; Žinić, B.; Piantanida, I. Fluorescent Analogues of FRH Peptide: Cu(II) Binding and Interactions with ds-DNA/RNA. *Chemosensors* **2022**, *10*, 34. https://doi.org/10.3390/chemosensors10010034

Academic Editors: Krzysztof Żamojć, Joanna Makowska and Dariusz Wyrzykowski

Received: 14 December 2021
Accepted: 12 January 2022
Published: 14 January 2022

1. Introduction

Many proteins base their biological activity on creating metal complexes [1–3]. Metals in proteins can form strong bonds that maintain the tertiary structure of proteins and can also bind to more than one polypeptide chain creating the quaternary structure of oligomers [4,5]. Besides their structural role, metals are also required for the function of metalloproteins [6]. For example, copper ions play an electron-transporting role based on their oxidation-reduction potential in mitochondrial cytochrome c oxidase [7], plastocyanins [8], superoxide dismutase [9] and other copper enzymes [10]. Peptides bind metal ions, in some cases very strongly, due to the presence of a large number of donor atoms. The binding of metals can be realized by the peptide backbone and also by donors present in amino acid side chains (Lys, Arg, Glu, Asp), the aromatic rings of amino acids (Phe, Tyr, Trp), and the imidazole group of histidine [11–14]. Additionally, several artificial His analogs [(4-thiazolyl)-l-alanine, (2-pyridyl)-l-alanine, and (pyrazol-1-yl)-l-alanine] can form similarly stable complexes with, e.g., copper cations [15].

For that particular reason, the histidine heterocycle attracted our attention, due to the structural similarity with 1,2,3-triazole and similar ability of both moieties to coordinate transition metal cations (for instance copper) [16,17]. Triazoles are easily accessible through copper(I) catalyzed 'click' chemistry (CuAAC), they are often used in peptides to mimic a *trans*-amide bond [18–20] and as an attractive bridging group to link two pharmacophores or attach fluorophores [21,22]. In a choice of fluorophores applicable to 'click' chemistry (CuAAC), we noticed that the well-known 3-azido-7-hydroxycoumarin is not fluorescent due to the emission quenching by the lone pair of electrons from the azido moiety [23].

However, after the CuAAC reaction and triazole ring formation, the obtained triazole-coumarin derivative is strongly emissive and can be used as a chemosensor for metal-ion detection [24,25]. Additionally, coumarin derivatives possess a wide range of biological activity [26,27] and show good fluorescent properties, which allows their use as markers in bioconjugate chemistry and fluorescent sensors [28,29].

In the presented research, starting from the Phe-Arg-His (FRH) peptide motif (Scheme 1), which is known as an efficient ligand for Cu^{2+}, and has a role in protecting synapses from copper-related oxidative damage by resisting ROS generation [30,31]; also belonging to the large family of short peptide sequences with a high affinity toward Cu^{2+} [32], we wanted to address two goals. First, prepare fluorescent FRH-peptide analogs with triazole replacing histidine and study their interactions with Cu^{2+} to see whether such analogs could replace FRH in biorelevant systems and allow easy and versatile "click" introduction of various fluorophores and other tools in the late-stage diversification of peptides/proteins. Second, to apply these FK(triazole) analogs as DNA/RNA targeting peptidoids for the recognition of double-stranded polynucleotide secondary structure and see if equipping peptidoids with Cu^{2+} will influence their DNA/RNA binding properties.

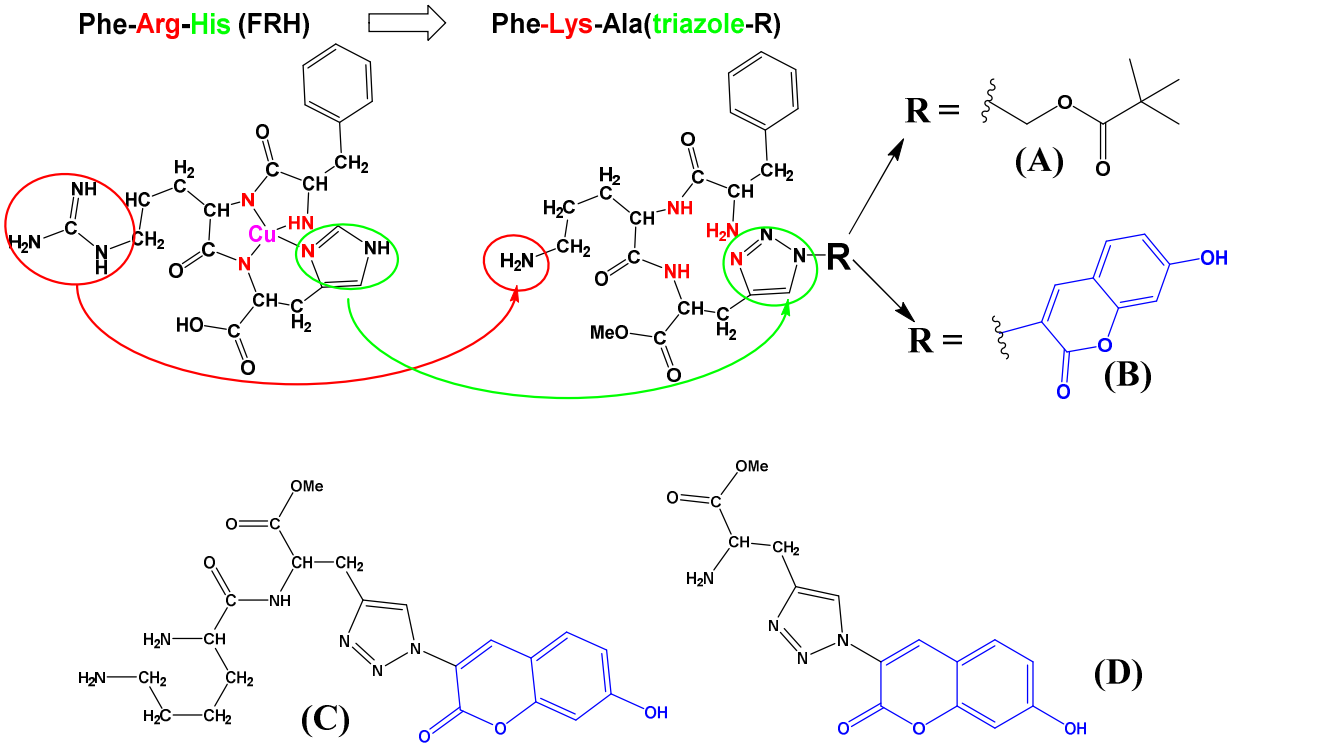

Scheme 1. Comparison of naturally occurring FRH peptide (drawn as a complex with Cu^{2+}) sequence with here designed and prepared FKA(triazole) analogs (**A**,**B**), and referent dipeptide (**C**) and amino acid (**D**). Red denotes replacement of Arg- with Lys-; green denotes replacement of Hys-imidazole- with triazole-; blue denotes coumarin chromophore.

We have designed and prepared the peptidoid Phe-Lys-Ala(triazole-Piv) analog **A**, its fluorescent (coumarin) analog **B** and corresponding referent compounds: dipeptide Lys-Ala(triazole-coumarin) (**C**, Scheme 1) and amino acid Ala(triazole-coumarin) (**D**, Scheme 1). We also replaced arginine with lysine (Scheme 1, denoted RED). Namely, lysine (Lys) and arginine (Arg) have been suggested to play similar biorelevant roles, and are both basic amino acids with high aqueous pK_a values (12−13.7 for Arg and ~10.5 for Lys) [33], allowing electrostatic interactions with anions at pH 7. In this case, lysine was more suitable due to easier protection by hydrophobic Boc-group (thus blocking Lys-amine protonation, see **B-boc**, Scheme 2), smaller steric volume and most importantly, ability to

form with targeted anionic DNA/RNA mostly electrostatic interactions, not complicated with additional H-bonding of Arg.

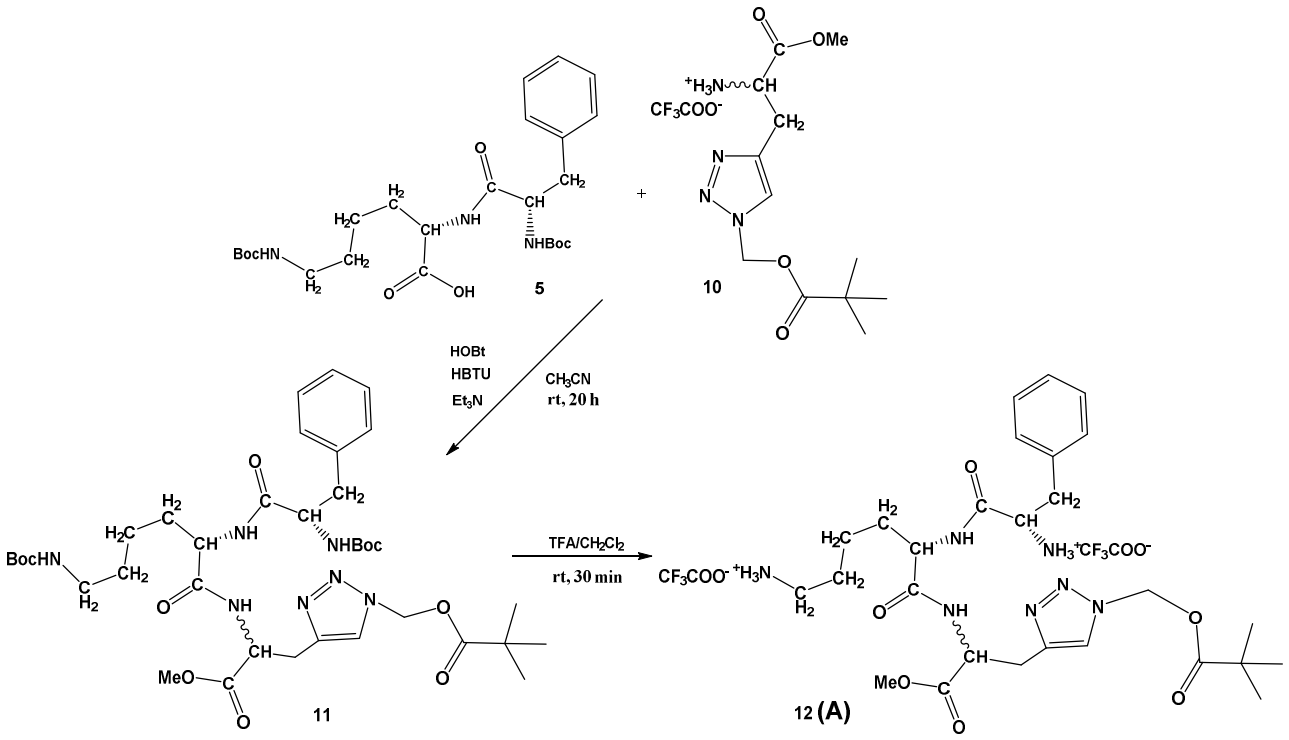

Scheme 2. Synthesis of Phe-Lys-Ala(triazole-Piv)-OMe conjugate **12** (**A**).

Novel peptidoids **A**, **B**, **C** due to the two positive charges of protonated amines, and in the case of coumarin substituent (**B**, **C**) also aromatic and hydrophobic interactions, are expected to interact non-covalently with ds-DNA/RNA, differing between various polynucleotide sequence secondary structures (Supplementary Materials, Table S1). We also tested the precursor of peptidoid **B** with both amines protected by Boc-groups (**B-boc**, see Scheme 2) to determine the importance of protonated amino groups for interactions with DNA/RNA. Moreover, peptidoids **A**, **B**, **C** should be able to strongly complex Cu^{2+} in an aqueous solution, and binding of such complexes to DNA/RNA could induce oxidative cleavage of nucleic acid backbone under temperature and pH-controlled conditions. Amino acid **D** serves as a fluorescent reference compound since it should not interact strongly with Cu^{2+} and due to its much smaller size should significantly differently interact with DNA/RNA.

2. Materials and Methods

2.1. General Information

Solvents were distilled from appropriate drying agents shortly before use. TLC was carried out on DC-plastikfolien Kieselgel 60 F254 and preparative thick layer (2 mm) chromatography was done on Merck 60 F254 plates (Merck KGaA, Darmstadt, Germany). (Merck, Merck KGaA, Darmstadt, Germany). NMR spectra were recorded on AV600 and AV300 MHz spectrometers (Bruker BioSpin GmbH, Rheinstetten, Germany), operating at 150.92 or 75.47 MHz for 13C and 600.13 or 300.13 MHz for 1H nuclei using DMSO-d_6 as the internal standard. Mass spectrometry was performed on the Agilent 6410 Triple Quad mass spectrometer (Agilent Technologies, Santa Clara, CA, USA) and high resolution mass spectra (HRMS) were obtained using a Q-Tof2 hybrid quadrupole time-of-flight mass spectrometer (Micromass, Cary, NC, USA).

All new peptidoids and their precursors were synthesized as briefly described in Schemes 2 and 3, and detailed synthetic description and full characterization are given in Supplementary Materials (Supplementary Materials, Schemes S1–S3).

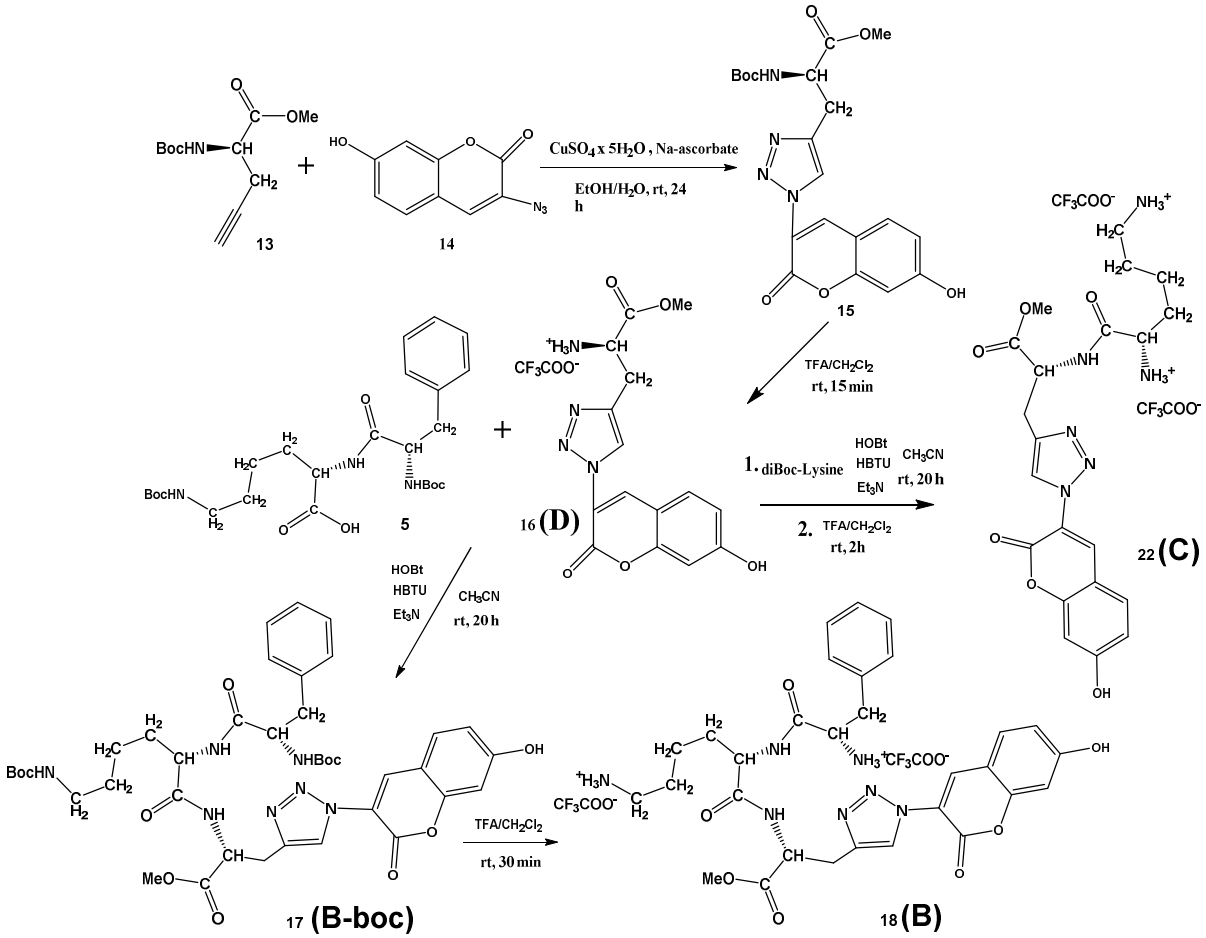

Scheme 3. Synthesis of Phe-Lys-Ala(triazole-coumarin) conjugate **B** (18), its Boc-protected precursor **B-boc** (17), Lys-Ala(triazole-coumarin)-OMe **C** (22) and referent coumarin amino acid **D** (16).

2.2. Spectrophotometric Measurements

All measurements were performed in aqueous buffer solution (pH = 7.0, c = 50 mM, sodium cacodylate buffer). The UV-Vis spectra were recorded on a Varian Cary 100 Bio spectrometer, fluorescence spectra were recorded on a Varian Cary Eclipse and Edinburgh FS5 fluorimeter. Circular dichroism (CD) spectra were recorded on JASCO J-815 spectropolarimeter at room temperature using 1 cm path quartz cuvettes with a scanning speed of 200 nm/min (an average of three accumulations). A buffer background was subtracted from each spectrum.

TC-SPC measurements were performed on an Edinburgh FS5 spectrometer equipped with a pulsed LED at 340 nm. The duration of the pulse was ≈800 ps. Fluorescence signals at 475 nm were monitored over 1023 channels with a time increment of ≈20 μs/1024 channels. The decays were collected until they reached 3000 counts in the peak channel. A suspension of silica gel in H_2O was used as a scattering solution to obtain instrument response function (IRF). Absorbances at 340 nm were 0.07–0.09. Before the measurements, the solutions were purged with a stream of nitrogen for 20 min. The measurement was performed at rt (25 °C). Decays of fluorescence were fitted to a sum of exponentials according to Equation (1):

$$R(t) = B_1 e^{-t/\tau_1} + B_2 e^{-t/\tau_2} + B_3 e^{-t/\tau_3} + B_4 e^{-t/\tau_4} \quad (1)$$

Using software implemented with the instrument; absolute quantum yields were determined by the Integrating sphere SC-30 of the Edinburgh FS5 spectrometer in the quartz cuvette of 10 mm path length, to avoid the scattering of incident light at the liquid-air interface, testing solutions with a 2 mL volume were used.

2.3. Study of DNA/RNA Interactions

Polynucleotides were purchased as noted: poly A—poly U and *calf thymus* (ct)—DNA (Sigma-Aldrich, Schnelldorf, Germany), and dissolved in sodium cacodylate buffer, c = 50 mM, pH = 7.0. The ct-DNA was additionally sonicated and filtered through a 0.45 mm filter to obtain mostly short (ca. 100 base pairs) rod-like B-helical DNA fragments. Polynucleotide concentration was determined spectroscopically by molar extinction coefficients supplied by the producer as the concentration of phosphates (corresponds to c(nucleobase)).

Thermal melting curves for ds-DNA, ds-RNA and their complexes with studied compounds were determined as previously described [34] by following the absorption change at 260 nm as a function of temperature. The absorbance of the ligands was subtracted from every curve and the absorbance scale was normalized. T_m values are the midpoints of the transition curves determined from the maximum of the first derivative and checked graphically by the tangent method. The ΔT_m values were calculated by subtracting the T_m of the free nucleic acid from the T_m of the complex. Every ΔT_m value here reported was the average of at least two measurements. The error in ΔT_m is $\pm$0.5 °C. It should be stressed that in experiments with Cu^{2+}-peptide complexes to referent DNA/RNA solutions, identical amounts of DMSO and Cu^{2+} were added and so obtained referent denaturation curves for DNA or RNA were used for the calculation of ΔT_m values caused by Cu^{2+}-peptide complexes.

3. Results

3.1. Synthesis

The dipeptide Boc-Phe-Lys(Boc)-OH **5** was prepared by known procedures, as described in Supplementary Materials (Scheme S1), as well as the protected *D*,*L*-propargylglycine **8** (Supplementary Materials, Scheme S2). Additionally, the conditions for the copper(I)-catalyzed azide-alkyne cycloaddition (CuAAC) were investigated and the best yield of protected Boc-Ala(triazole-Piv)-OMe **9** (93%) was obtained by an in situ azidation/cycloaddition protocol [35,36] from compound **8** using sodium azide, chloromethyl pivalate, and the sodium ascorbate, CuI, DMEDA/EtOH, H_2O system. The Boc-protecting group was removed with a mixture of CH_2Cl_2/TFA, affording **10** in quantitative yield (Supplementary Materials, Scheme S2). The Ala(triazole-Piv)-OMe **10** was coupled with dipeptide Boc-Phe-Lys(Boc)-OH **5** under standard HBTU/HOBt conditions, providing tripeptide, Boc-Phe-Lys(Boc)-Ala(triazole-Piv)-OMe **11**, in moderate 37% yield. Finally, Boc removal from **11** was again carried out with TFA, providing Phe-Lys-Ala(triazole-Piv)-OMe conjugate **12** (**A**) in quantitative yield (Scheme 2).

Finn et al. [37] performed solid-state synthesis and selection for oligopeptide-based CuAAC catalysts, using peptide libraries, different terminal alkynes, and 3-azido-7-hydroxycoumarin. In the CuAAC reaction of 3-azido-7-hydroxycoumarin with a library of peptides and propargyl glycine as the terminal alkyne, only low yields (0–25%) were achieved. Contrary, the "click" reaction of the protected *D*-propargylglycine **13** with 3-azido-7-hydroxycoumarin **14** in the presence of copper(II) sulfate and sodium ascorbate at room temperature gave an excellent yield of 81% on desired Boc-Ala(triazole-coumarin)-OMe conjugate **15**, which precipitated from the reaction mixture and was isolated by recrystallization from methanol (Scheme 3). After deprotection of the Boc group in TFA/CH_2Cl_2, the conjugate **16** was isolated in quantitative yield. Finally, standard coupling reaction between dipeptide Boc-Phe-Lys(Boc)-OH **5** and the conjugate **16** using HBTU/HOBt coupling reagents and triethylamine in acetonitrile gave protected fluorescent Boc-Phe-Lys(Boc)-Ala(triazole-coumarin)-OMe **17 (B-boc**) in the 76% yield. Again, the Boc-protecting groups

were removed with a mixture of TFA/CH_2Cl_2, affording Phe-Lys-Ala(triazole-coumarin)-OMe **18** (**B**) conjugate in the 97% yield. The Lys-Ala(triazole-coumarin)-OMe **22** (**C**) can be prepared by two alternative routes, either from **D** reacting with diBoc-protected lysine (Scheme 3) or coupling first *D*-propargylglycine **D-7** with diBoc-protected lysine and then "clicking" 3-azido-7-hydroxycoumarin **14** (Supplementary Materials, Scheme S3). Latter "click" reaction performed in the presence of copper(I) iodide and DIPEA at room temperature gave an excellent yield of 91% on desired Lys-Ala(triazole-coumarin)-OMe **21**, demonstrating that "click" reaction can be performed in the late-stage diversification of peptides.

3.2. Photophysical Characterization

The studied peptides **A**, **B**, **B-boc**, **C**, **D** were moderately soluble in water, thus for easier handling the stock solutions were prepared in DMSO (5 mM), stored at +8 °C and for further experiments aliquots diluted in an aqueous solution before the experiment.

The absorbances of buffered solutions at pH 7 of studied compounds are proportional to their concentrations up to $c = 2 \times 10^{-5}$ M (Supplementary Materials, Figures S1–S5). All studied coumarin derivatives emit fluorescence with an emission maximum at about 475 nm, emission intensity proportional to their concertation up to $c = 2 \times 10^{-6}$ M (Supplementary Materials, Figures S9, S11, S13 and S14). Absorption maxima, corresponding molar extinction coefficients and excitation and emission maxima are given in Table 1.

Table 1. Electronic absorption and emission data of **B**, **B-boc**, **C** and **D** at pH 7, sodium cacodylate buffer, c = 50 mM.

Compd.	λ_{max}/nm	ε/M^{-1}cm^{-1}	[b] Φ_f	[a] λ_{exc}/nm	[a] λ_{em}/nm	τ/ns [a] (purged)	χ2
A	266	5826 ± 60	c	c	c	c	c
B	392	11,633 ± 167	0.77 ± 0.05	340 405	477	4.36 (100%) 4.32 (100%)	1.062 1.040
B-boc	353	12,620 ± 60	0.36 ± 0.05	340 405	476	4.47 (100%) 0.49 (5.84%) 4.40 (94.16%)	1.055 0.933
C	393	11,262 ± 496	0.58 ± 0.05	340 405	475	4.22 (100%) 4.21 (100%)	1.082 1.079
D	353	15,479 ± 106	0.45 ± 0.05	340 405	472	4.20 (100%) 4.19 (100%)	1.009 1.032

[a] Water solutions were purged by Argon, samples were excited by pulsing diodes at 340 nm and 405 nm, to study neutral and anionic tautomer, respectively. The measurements were performed three times and the average values are reported. The associated errors correspond to the maximum absolute deviation; [b] Absolute fluorescence quantum yield was determined by integrating sphere SC-30, Edinburgh Inst., for Argon purged solutions, by λ_{exc} = 353 nm. [c] Nonfluorescent at experimental conditions.

The UV/Vis spectra of 7-hydroxycoumarin and its derivatives are pH-dependent due to the two tautomeric forms [38]. We repeated the experiment by collecting UV/Vis spectra of referent amino acid coumarin **D** at various pH (Figure 1a, pH = 5.0, 7.0 and 8.7) and got comparable results, thus attributing particular UV/Vis spectra to the dominant form of the corresponding tautomer. The fluorescence excitation spectra of **D** show comparable dependence on pH (Figure 1). Other coumarin peptidoids (**B**, **B-boc**, **C**) showed comparable changes in UV/Vis spectra (Supplementary Materials, Figures S6–S8), pointing out universal responsiveness of coumarin tautomerism. Surprisingly, we noticed that heating solutions of all studied coumarin derivatives resulted in changes of their UV/Vis spectra (Figure 1b) comparable to pH-dependence (Figure 1c). To the best of our knowledge, such temperature dependence of coumarin tautomerism was not reported previously. Since temperature dependent experiments were done in a buffered solution, pH 7.0, buffer keeping the pH constant during heating, the observed change of the UV/Vis spectrum could be

attributed to the shift of coumarin tautomeric equilibrium toward anionic species, caused likely by temperature-sensitive electronic distribution within aromatic system.

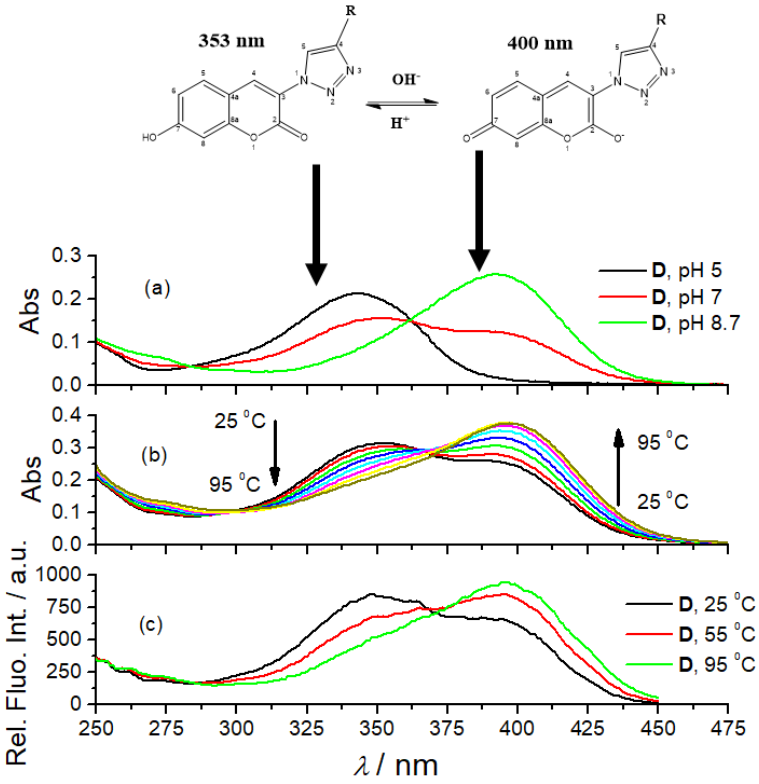

Figure 1. The dependence of amino acid coumarin **D** UV/Vis spectra ($c = 2 \times 10^{-5}$ M) on pH (**a**); temperature (**b**); and pH dependence (**c**) of **D** fluorescence excitation spectra ($c = 1 \times 10^{-6}$ M, $\lambda_{em} = 475$ nm).

Furthermore, a comparison of the UV/Vis spectra of **B**, **B-boc**, **C** and **D** collected at pH 7 (Figure 2) revealed the dominant maximum of **B-boc** and **D** at 353 nm attributed to neutral coumarin tautomer, while the dominant maximum of **B** and **C** at 400 nm was attributed to anionic coumarin tautomer. Only **B** and **C** have protonated, thus positively charged ε-amine of lysine, which could be intramolecularly folded-back to interact with anionic tautomer of coumarin, correspondingly shifting tautomeric equilibrium and causing an increase of the maximum at 400 nm.

We also tested the dependence of fluorescence emission spectra of **B**, **B-boc**, and **D** on pH and temperature, which revealed that amino acid coumarin **D** and hydrophobic boc-protected **B-boc** emission is enhanced with temperature increase, at variance to **B**, which emission is decreased (Supplementary Materials, Figures S10, S12 and S15). Again, such difference in emission response could be related to tautomeric equilibrium discussed for UV/Vis spectra (Figure 2).

Further, we also studied in detail the fluorimetric properties of **B**, **B-boc**, **C** and **D** in an aqueous medium by the characterization of singlet excited state lifetimes utilizing time-correlated single-photon counting (TC-SPC; Table 1). The samples were excited by pulsing diodes at 340 nm and 405 nm, to study neutral and anionic tautomer, respectively, and the emission was detected at 475 nm. Fluorescence decays were fitted to single exponential functions, giving very similar lifetimes in the range 4.2–4.5 ns, irrespectively on excitation wavelength used. Only for **B-boc** excited at 405 nm, fluorescence decay was best described as the sum of two exponentials, with a small contribution of a shorter decay component. Thus, the emission mechanism of neutral and anionic tautomers does not differ significantly under the experimental conditions used.

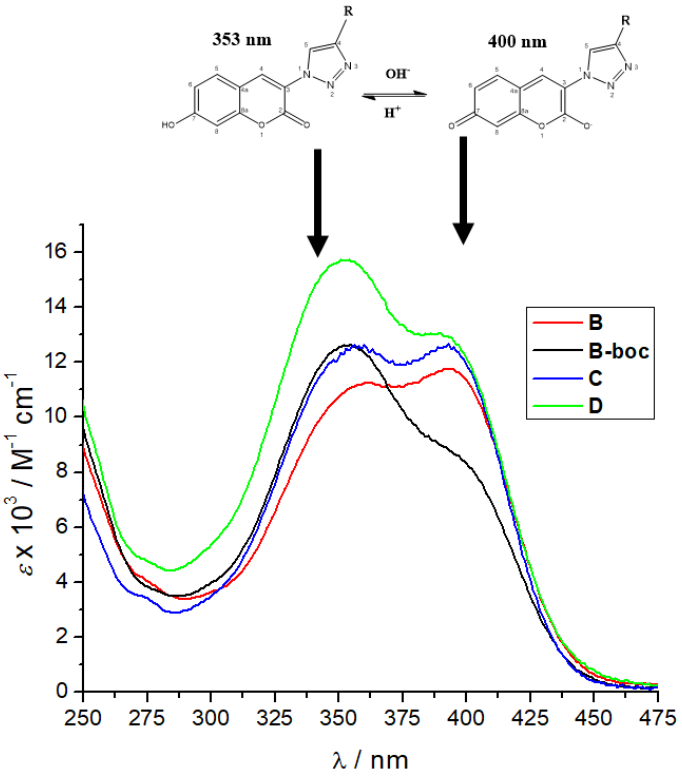

Figure 2. Comparison of UV spectra **B**, **B-boc**, **C** and **D** at pH 7, sodium cacodylate buffer, *c* = 50 mM.

Fluorescence quantum yields of **B**, **B-boc**, **C** and **D** were quite high (Table 1), as expected for the quinolone fluorophore. The fluorescence quantum yields of **B** and its close analog **B-boc** significantly differ, while molar extinction coefficients are almost the same. However, only for **B-Boc** short-lived fluorescence decay component was observed (Table 1), suggesting the presence of an additional relaxation pathway for the excited molecule, which could be responsible for a significant decrease of quantum yield. For the accurate analysis of emission decay pathways, an extensive computational analysis would be necessary, extending out of the scope of this bio-target oriented research.

3.3. Binding of Cu^{2+} Cation

As described in the Introduction and shown in Scheme 1, the studied peptidoids **A**, **B**, **B-boc** and **C** should strongly bind Cu^{2+} cation, while **D** due to the fewer metal coordination sites (only two) could form a less stable complex.

Since for all compounds triazole ring is expected to participate in the coordination of Cu^{2+}, such interaction will likely influence the coumarin directly attached to triazole. Indeed, the addition of $CuCl_2$ changed the UV/Vis spectra of coumarin-analogues **B**–**D** (Supplementary Materials, Figure S16), whereby there was again the significant difference between the response of **B-boc** (only peptidoid with Boc-protected amino groups, the hypochromic effect at 353 nm) in respect to **B** and **C** (selective hyperchromic effect at 400 nm) and referent **D**, decreasing at 353 nm and increasing at 400 nm. The reason why the addition of Cu^{2+} cation to any peptidoid with a free amino group (**B**, **C**, **D**), increases the maximum attributed to the coumarin anionic tautomer (400 nm, see Figure 2) cannot be accurately determined only from UV spectra changes, and NMR studies were hampered by the paramagnetic nature of the Cu^{2+} cation.

However, UV/Vis titrations did not allow the collection of enough data points for the accurate calculation of binding constants. Therefore, we took advantage of **B**, **B-boc**, **C** and **D** intrinsic fluorescence and performed fluorimetric titrations. The addition of Cu^{2+} cation strongly quenched emission of both, **B**, **B-boc**, even at 10 nM concentrations (Figure 3), suggesting very high binding affinity. Processing of the titration data by the

Specfit program for multivariate analysis [39,40] yielded as the only solution, the formation of two complexes; peptidoid (**B**, **B-boc**): Cu^{2+} = 1:1 and 2:1 stoichiometry.

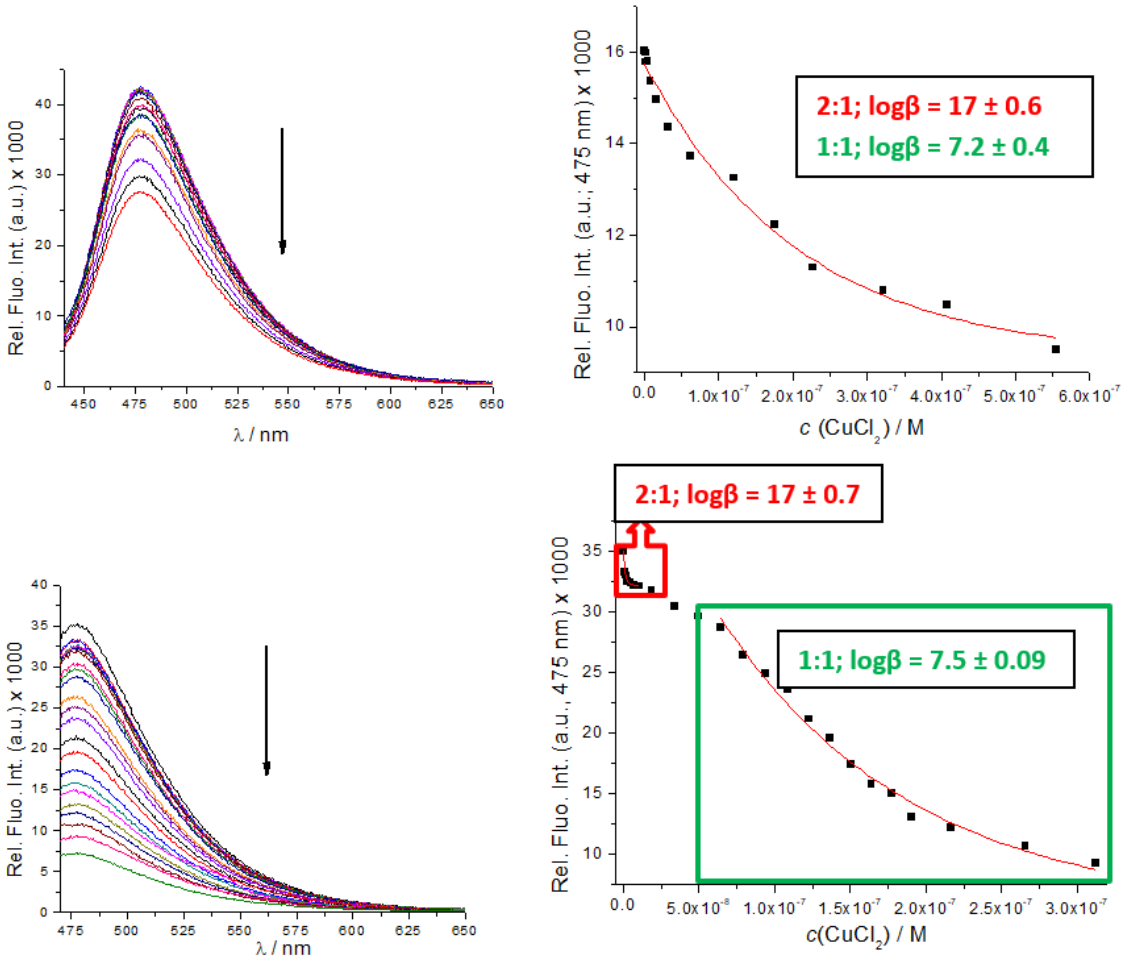

Figure 3. Fluorimetric titrations of **B-boc** (**up**) and **B** (**down**) ($c = 1 \times 10^{-8}$ M; λ_{exc} = 353 nm) with $CuCl_2$. RIGHT: dependence of fluorescence at λ_{max} = 475 nm on $c(CuCl_2)$. Done at pH 7, sodium cacodylate buffer, c = 50 mM.

Titration of **C** with $CuCl_2$ resulted in similar emission quenching but fitting showed that a 1:1 complex was formed, (Supplementary Materials, Figure S17), with a binding constant log$K$ = 6.9 M^{-1}, very similar to corresponding (1:1 stoichiometry) binding constants determined for **B** and **B-boc** (Figure 3). Obtained binding constants are roughly in accordance with the affinity of similar peptide sequences [32,41], usually varying between log$K$ = 8–12 M^{-1}.

When complexed with Cu^{2+}, fluorescence lifetimes of coumarin fluorophores in **B**, **B-boc** and **C** (Supplementary Materials, Table S1) did not change significantly, suggesting a static quenching mechanism.

Peptidoid **A** is non-fluorescent, therefore, we performed a competitive experiment, by preparing **C**/Cu^{2+} complex and then extracting Cu^{2+} by additions of **A**, monitored by the resulting emission increase of **C** (Figure 4, Supplementary Materials, Figure S18). Results clearly show that **A** very efficiently extracted Cu^{2+} from **C**/Cu^{2+} complex, calculated ratio $r[C]/[A]_{50\%}$ = 0.35 suggesting similar binding affinity of **A** and **C**.

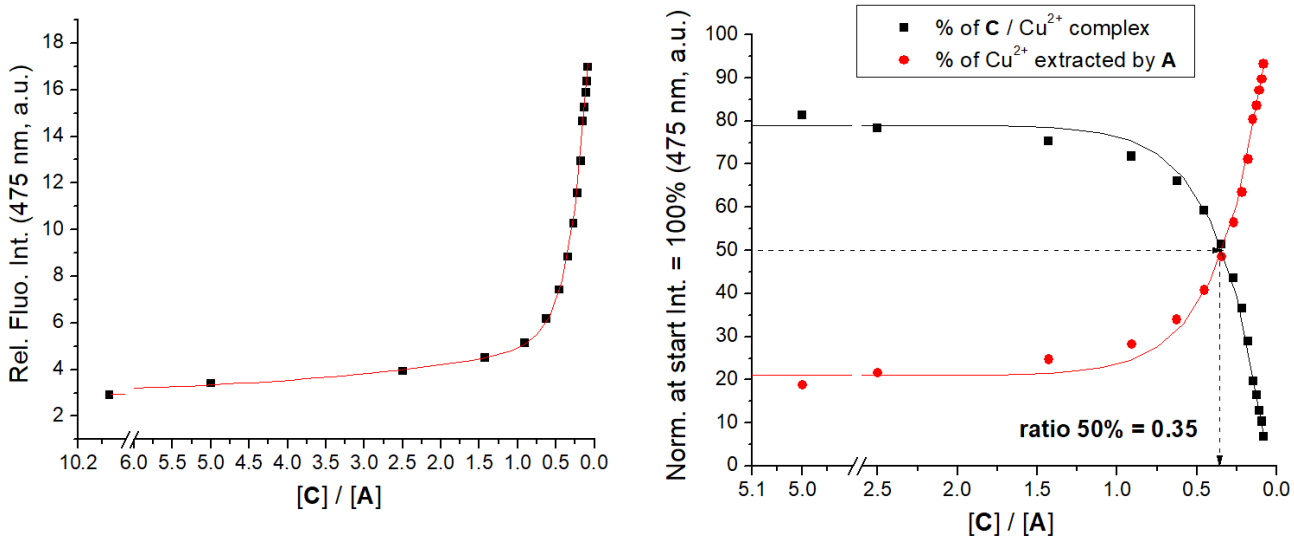

(**a**) (**b**)

Figure 4. (**a**) Changes in fluorescence of **C** ($c = 1 \times 10^{-6}$ M, λ_{exc} = 353 nm, λ_{em} = 475 nm) in the complex with $CuCl_2$ ($c = 1 \times 10^{-6}$ M) upon addition of **A**; (**b**) the percentage of **C** or Cu^{2+} released from the **C**/Cu^{2+} complex. Done at pH 7.0; sodium cacodylate buffer, c = 50 mM.

Further, coumarin peptides are chiral and should possess CD spectra, however, due to the distance between the asymmetric center of amino acids and the coumarin chromophore and flexibility, their CD bands are expected <210 nm. We used DMSO for stock-solution preparation to ensure solubility of hydrophobic **B-boc**, and also DMSO is a common bio-applicable solvent for biological testing, we could collect CD spectra only at >240 nm range. Under such conditions, none of the studied peptidoids showed a measurable CD spectrum (Figure 5, Supplementary Materials, Figure S19).

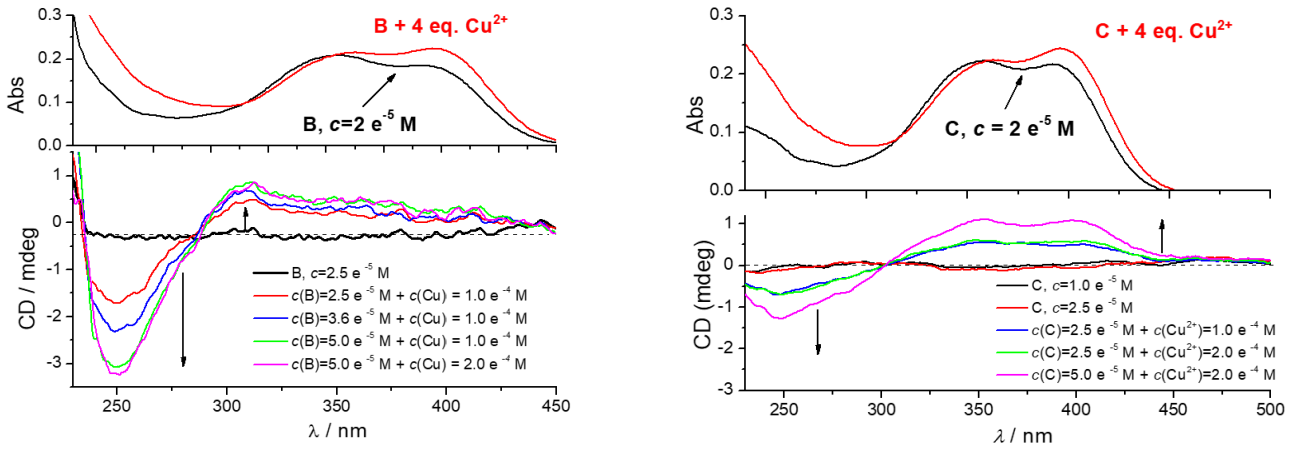

Figure 5. Effect of $CuCl_2$ addition to CD spectra of **B** (**left**) or **C** (**right**). The UV/Vis spectra given at the top are taken from experiments given in Supplementary Materials, Figure S16. Done at pH 7, sodium cacodylate buffer, c = 50 mM.

However, the addition of $CuCl_2$ resulted in the appearance of a strong bisignate induced ICD spectrum of **B** and **C** in the 240–450 nm range (Figure 5), with intensity proportional to the increasing c(**B** or **C**). The shape and intensity of ICD spectra of **B**/Cu^{2+} or **C**/Cu^{2+} complexes are very similar, therefore the lack of phenylalanine in **C** is not essential for chiral folding of peptidoid. The **B-boc** surprisingly did not show a measurable ICD spectrum (Supplementary Materials, Figure S19). The fact that the only difference between **B** and **B-boc** are free amino groups of the former peptidoid (**B**), supported the

conclusion that free amino groups take a prominent part in the chiral folding of a peptidoid around Cu^{2+} cation. As expected, referent amino acid **D** could not fold around Cu^{2+} cation and showed no ICD bands. Similarly, no ICD bands were observed for the peptidoid **A**/Cu^{2+} complex, due to the lack of chromophore (coumarin) (Supplementary Materials, Figure S19).

The ICD bands agree well with the UV spectrum of coumarin (Figure 5), thus a negative band with a maximum at 250 nm coupled with a positive CD band at 280–450 nm could be attributed to the mutually orthogonal transition moment vectors of coumarin chromophore oriented in a chiral space. Only detailed computational analysis can deconvolute spectral composition of observed induced CD spectrum of **B**/Cu^{2+} or **C**/Cu^{2+} complex, taking into account structural properties of **B** or **C**, as well as lack of corresponding ICD spectra for other peptidoids. However, the observed (I)CD spectrum of **B**/Cu^{2+} or **C**/Cu^{2+} complex could be attributed to the intramolecular folding of peptides around the Cu^{2+} cation, orienting coumarin in a chiral space, and thus giving rise to the secondary structure of strong chirality. Such sensitivity of CD spectrum toward molecular conformation is well-documented [42], and was extensively used to probe or induce chiral space for analytical or sensing purposes [42–44].

Thus, peptidoids **B** and **C** can be considered as highly sensitive CD probes for the binding of Cu^{2+} cations, encouraging further studies with other metal cations.

3.4. Study of Interactions of **A**, **B**, **B-boc**, **C** *and* **D** *with ds-DNA and ds-RNA*

3.4.1. Thermal Denaturation Experiments

The thermal denaturation experiments provide information about the ds-polynucleotide helix thermal stability as a function of interaction with added small molecules and the difference between the T_m value of free ds-polynucleotide and a complex with a small molecule (ΔT_m value) is an important factor in the characterization of small molecule/ds-polynucleotide interactions [34].

Thermal denaturation experiments revealed that the addition of **A**, **B**, **B-boc**, **C** and **D** did not stabilize ct-DNA or ds-RNA against thermal denaturation (Supplementary Materials, Figures S29 and S30), with exception of **C**, which weakly destabilized only ds-RNA. However, if **A**–**D** peptidoids were before thermal denaturation experiments pre-incubated 2 min. with a 4-fold excess of Cu^{2+} ($CuCl_2$), such complexes stabilized ds-DNA and strongly stabilized ds-RNA (Table 2, (Supplementary Materials, Figure S31) in comparison to ds-DNA/RNA with added only Cu^{2+} cation.

Detailed analysis of thermal denaturation results revealed that all peptidoid/Cu^{2+} complexes stabilized ct-DNA similarly, and the same non-selectivity was observed for ds-RNA. Thus, the structure of peptidoids did not influence the thermal stabilization effect, and most importantly, even amino acid **D** with only two coordination sites for Cu^{2+} was similarly effective as longer peptidoids. Such equal effect implies that the Cu^{2+} cation is not fully immersed in the complex with **A**, **B**, **B-boc,** or **C**, but eventually during the process of binding to DNA/RNA is partially exposed to the polynucleotide. In that way Cu^{2+} cations can form additional electrostatic or metal coordination interactions to phosphate backbone or nucleobases, respectively, stabilizing DNA/RNA double helix against thermal denaturation.

Table 2. Thermal denaturation ([a] ΔTm/°C) of ct-DNA (c(ct-DNA) = 2.5 × 10^{-5} M, $r_{[(compd.)]/[ct\text{-}DNA]}$ = 0.3) and poly A poly U (c(RNA)= 2.5 × 10^{-5} M, $r_{[(compd.)]/[poly\ A\ poly\ U]}$ = 0.3) at pH 7.0 (sodium cacodylate buffer, c = 50 mM) upon addition of **A**, **B**, **B-boc**, **C** and **D**, or addition of pre-prepared complexes of **A**, **B**, **B-boc**, **C** with four equivalents of Cu^{2+}.

Compound	ctDNA	Poly A–Poly U
A	0	0
[b] **A** + $4Cu^{2+}$	+3.7	[c] 0; +9.5
B-boc	0	0
[b] **B-boc** + $4Cu^{2+}$	+2.7	[c] 0; +10.3
B	0	0
[b] **B** + $4Cu^{2+}$	+2.0	[c] 0; +11.6
C	0	−2.5
[b] **C** + $4Cu^{2+}$	+2.0	[c] 0; +11.0
D	0	0
[b] **D** + $4Cu^{2+}$	+2.5	[c] 0; +8.5

[a] Error in [a] ΔTm: ± 0.5 °C; [b] The complex of peptidoids **A**-**C** (for ratio r = 0.3) with 4 equivalents of Cu^{2+} was prepared in cuvettes and after 2 min. of equilibration DNA or RNA was added and incubated at room temp. for 2 min. before thermal denaturation experiment. To control DNA/RNA solution identical amounts of DMSO and Cu^{2+} were added and so obtained denaturation curves were used for the calculation of ΔTm values. [c] Biphasic denaturation curves, suggesting that at given ratio r, not complete RNA is saturated with studied peptidoid/Cu^{2+} complex, containing denaturation of non-affected parts of RNA (ΔTm = 0) and thermally stabilized sections (ΔTm = 8–11 °C).

3.4.2. Spectrophotometric Titrations

UV/Vis titrations: The addition of ct-DNA yielded minor hypochromic changes in the UV/Vis spectra of coumarin-analogs (**B**, **B-boc**, **C**) and negligible effect on the UV/Vis spectrum of **D** (Supplementary Materials Figure S20). Intriguingly, the addition of ct-DNA to the previously prepared Cu^{2+}/**C** complex also resulted in measurable hypochromic effect in 300–450 nm range, allowing estimation of binding constant about logKs = 5.2 (Supplementary Materials, Figure S21, LEFT; down). However, changes in the UV/Vis spectra were too small for accurate calculation of binding constants. Therefore, taking advantage of most of the intrinsic fluorescence of studied compounds (**B**, **B-boc**, **C** and **D**), we performed fluorimetric titrations with various ds-DNA and ds-RNA to assess the binding stability of non-covalent complexes formed.

The addition of any ds-DNA or ds-RNA to **B**, **B-boc**, **C** resulted generally in quenching of their emission, (Figure 6, Table 3, Supplementary Materials Figures S22–S24), at variance to amino acid analog **D**, for which fluorescence did not change (Supplementary Materials, Figure S25), which agreed well with UV/Vis titrations (no change in the UV/Vis spectrum of **D**). This result strongly supported the essential contribution of at least the dipeptide sequence attached to coumarin for efficient interaction with ds-DNA/RNA, whereas **D** due to the too weak binding interactions did not form a measurable percentage of a non-covalent complex with DNA/RNA. The reason for emission quenching of **B**, **B-boc**, **C** coumarin upon binding to DNA/RNA is not aromatic stacking interaction with nucleobases by intercalation, since such binding mode should yield a strong thermal stabilization effect, which was not observed for **B**, **B-boc** or **C** (Table 2). Thus, **B**, **B-boc**, **C** bind to ds-DNA/RNA likely by insertion into grooves, within which numerous binding interactions are established (H-bonding, hydrophobic effect, Van der Waals interactions, electrostatic interactions of positively charged amines of **B** or **C** with DNA/RNA phosphates). In such a hydrophobic binding site, the coumarin fluorophore is not exposed to the water, which could influence its tautomer equilibrium and also coumarin could form edge-to-edge aromatic interactions with nucleobases (allowing energy transfer relaxation), all of which as a cumulative effect, yields emission quenching.

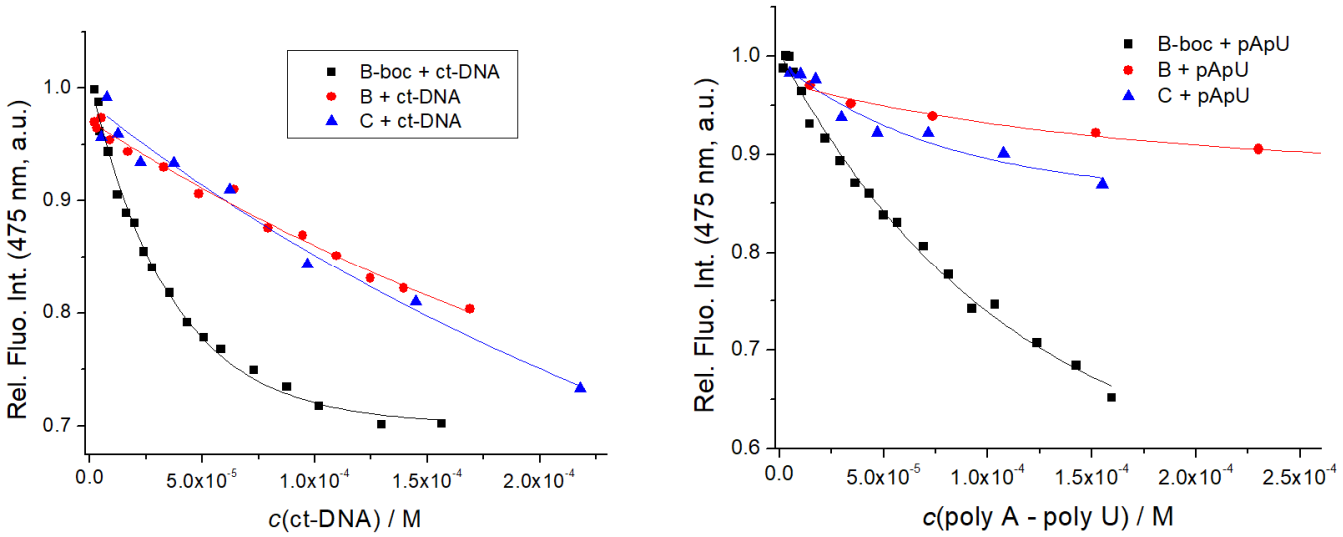

Figure 6. Fluorimetric titration of **B**, **B-boc**, **C** ($c = 1 \times 10^{-6}$ M; λ_{exc} = 353 nm) with ct-DNA and poly A–poly U: dependence of fluorescence at λ_{max} = 475 nm on *c*(DNA, RNA). Done at pH 7, sodium cacodylate buffer, *c* = 50 mM.

Table 3. Binding constants (log K_s) [a] and spectroscopic properties of complexes of conjugates **B**, **B-boc, C**, **D** with ds-polynucleotides calculated by processing fluorimetric titrations, done at pH = 7, sodium cacodylate buffer, *c* = 50 mM.

Compound	ct-DNA	poly A–poly U
B-boc	5.4	5.7
B	4.3	3.8
C	<4 [b]	4.8
D	b	b

[a] Processing of titration data by means of Scatchard equation [45] gave values of the ratio *n*[bound dye]/[polynucleotide] = 0.1 and 0.3. For easier comparison, all log K_s values were re-calculated for fixed *n* = 0.2. Correlation coefficients were >0.99 for all calculated values of log K_s. [b] Too small changes for accurate calculation of binding constants.

Titration data were by non-linear regression, fitted to the Scatchard equation [45], yielding the binding constants (Table 3). Intriguingly, emission of highly hydrophobic and neutral **B-boc** was significantly stronger quenched by ds-DNA/RNA in comparison to its dicationic, hydrophilic analog **B** or dipeptide **C**, and moreover, the affinity of **B-boc** was at least order of magnitude stronger (Table 3) in comparison to dicationic analogs **B** or **C**. Such results imply that hydrophobic interactions of highly hydrophobic and neutral **B-boc** are dominant in DNA/RNA binding, whereas electrostatic interactions of positively charged amines of **B** or **C** do not contribute significantly.

In order to estimate the DNA-affinity of non-emissive **A**, we opted for Indicator Displacement Assay (IDA) methodology [46], by preparing **B-boc**/ct-DNA complex (as shown in Figure 6, in which **B-boc** emission is partially quenched) and then displacing **B-boc** by addition of **A**, monitoring simultaneously, the eventual recovery of **B-boc** emission. A similar competition strategy proved to be successful for the determination of A/ Cu^{2+} binding (Figure 4). However, even 20-fold excess of **A** over **B-boc** did not increase **B-boc**/ct-DNA complex emission, suggesting that **A** affinity toward ct-DNA is negligible. This result indicated the importance of coumarin for the **B**, **B-boc**, **C** binding to DNA or RNA, likely due to the hydrophobic and eventual H-bonding interaction within DNA/RNA grooves.

We tried to perform fluorimetric titrations of pre-prepared **B-D**/Cu^{2+} complexes (2:50 μM ratio to ensure >90% of complex formed) with ct-DNA (ratios 0.13–0.01), but only negligible changes in emission were observed. Such insensitivity of coumarin emission could be attributed to the fact that both, Cu^{2+} and DNA cause similar fluorescence quench-

ing. Only **B-boc**/Cu^{2+} complex emission showed weak but measurable changes for the collection of three data points, allowing rough estimation of binding affinity log*Ks* ~ 5 M^{-1}.

3.4.3. Circular Dichroism (CD) Experiments

To investigate the mode of binding of peptides **B**-**D** to ct-DNA and poly A–poly U in more structural detail, we used circular dichroism (CD) spectroscopy. CD spectroscopy is a useful analytical tool in the binding study of small molecules to chiral macromolecules, such as DNA [47] since it can provide information on the binding mode to a polynucleotide, with distinctive spectral differences for intercalators and groove binding derivatives [48]. Peptides **A**-**D** are chiral; however, they show no measurable CD bands within the 240–400 nm range (Supplementary Materials, Figures S26–S28), thus not interfering with CD bands of DNA/RNA in 240–290 nm range, nor with eventual induced ICD bands of coumarin, which could appear within the 300–400 nm range upon binding to ds-DNA/RNA.

The addition of **B**-**D** in both the absence or presence of Cu^{2+} cation, to any used ds-DNA or ds-RNA, didn't influence significantly the CD spectrum of a polynucleotide, thus suggesting that the helical structures of ds-DNA or ds-RNA remained unperturbed by the binding of peptidoids. Additionally, no ICD bands >300 nm were observed, thus suggesting non-uniform orientation of coumarin units in respect to the polynucleotide chiral axis [48]. In the particular case of the CD spectrum of the **B**/Cu^{2+} complex (Figure 5), the addition of DNA did not cause any significant change, thus suggesting the preservation of the structure of the **B**/Cu^{2+} complex, when it is bound to ds-DNA. Taking into account the volume of self-folded **B**/Cu^{2+} complex and the possible binding sites on ds-DNA, insertion into the DNA minor groove is the only plausible binding option.

4. Discussion and Conclusions

We prepared four novel peptidoids, three of them based on to Phe-Arg-His (FRH) peptide sequence, modified by the replacement of histidine with triazole and arginine with lysine. Three of those peptidoids were equipped with a fluorophore, coumarin, which showed pH-dependent UV/Vis and fluorescence spectra, attributed to well-known coumarin tautomerism but similar changes were observed also upon the heating of buffered solution (pH 7.0), suggesting that temperature increase shifts the coumarin tautomeric equilibrium toward anionic species.

Intriguingly, UV/Vis spectra showed that only peptidoids with free amino groups of lysine side-chain (**B**, **C**) shift coumarin tautomeric equilibrium slightly toward anionic tautomer, thus suggesting intramolecular interaction between anionic coumarin and cationic protonated amine. All coumarin analogs showed high molar extinction coefficients and mostly single exponential emission decay independent on tautomerism, thus behaving as promising chromophores/fluorophores.

The addition of Cu^{2+} cation caused changes in UV/Vis spectra of coumarin analogs **B**–**D** and emission of all coumarin-peptidoids was strongly quenched by the addition of Cu^{2+} cation by static quenching mechanism (supported by no change in emission decay lifetime). Competitive experiments demonstrated that non-fluorescent Phe-Lys-triazole peptidoid analog (**A**, lacking coumarin), also strongly binds Cu^{2+} cations. These novel Phe-Lys-A(triazole) peptidoids (**B**, **B-boc**) retained strong, nanomolar affinity toward Cu^{2+} cations, typical or FRH peptides and similar motifs [32,41], thus demonstrating that triazole can efficiently replace histidine as a copper-coordinating moiety. Moreover, even shorter Lys-A(triazole) peptidoid **C** showed a strong, sub-micromolar, binding constant for the Cu^{2+} cation, although it has only three Cu-coordination sites, in that way leaving free a coordination site for another ligand. Most intriguingly, only Phe-Lys-A(triazole)coumarin **B** and its shorter analog Lys-A(triazole)coumarin **C**; both with a free amino group, exhibited strong induced CD spectrum upon Cu^{2+} binding. Such a chiral response was attributed to the intramolecular folding of peptidoid **B** or **C** around the Cu^{2+} cation leading to the chiral positioning of coumarin, at variance to other peptidoids lacking either coumarin or free amino groups essential for chiral folding. Thus, the Lys-A(triazole)coumarin unit can be

considered as the shortest peptidoid sequence with highly sensitive fluorescent and chiral CD response for the Cu^{2+} cation, encouraging further studies with other metal cations.

Studied Phe-Lys-A(triazole)coumarin-peptidoids (**B**, **B-boc**) bind to ds-DNA and ds-RNA by moderate, 10-micromolar affinity, while Lys-A(triazole)coumarin **C** affinity was at least an order of magnitude lower, and coumarin –amino acid (**D**) or Phe-Lys-A(triazole) (**A**) did not show measurable interaction with DNA/RNA. Thus, full Phe-Lys-A(triazole) sequences and coumarin are necessary for efficient DNA/RNA binding, most likely controlled by a set of hydrophobic, H-bonding and/or electrostatic interactions. Peptidoids bind within the ds-DNA minor groove or ds-RNA major groove, since only these biding sites have the adequate size and hydrophobicity for small-molecule accommodation (Supplementary Materials, Table S2). Very intriguingly, only complexes of all studied peptidoids with Cu^{2+} strongly stabilize ds-DNA/RNA, supporting significant involvement of Cu^{2+} cations in the interaction within the polynucleotide binding site. Here collected data do not show whether this additional binding is related to Cu^{2+} electrostatic interaction with negatively charged phosphate backbone or Cu^{2+} is partially coordinated by heterocyclic nucleobases or sugar moieties. The application of NMR was hampered by the paramagnetic properties of Cu^{2+}, thus future studies will be focused on the crystallization of peptidoid/Cu^{2+} systems and their complexes with DNA. In addition, if a Cu^{2+} cation is brought in the vicinity of the DNA backbone, it can cause oxidative cleavage of the DNA, thus here presented peptidoids could act as artificial endonucleases. For that reason, here the presented results strongly encourage future research focused on the further optimization of peptidoid structure and DNA-cleavage studies in biorelevant conditions, combined with human cell uptake and intracellular distribution.

Supplementary Materials: The following are available online at https://www.mdpi.com/article/10.3390/chemosensors10010034/s1, additional photophysical characterization in an aqueous medium (UV/Vis and fluorimetric data, Figures S1–S15), additional data on interactions with Cu^{2+} cation (UV/Vis, fluorimetric and CD data, Figures S16–S19, Table S1), DNA and RNA (UV/Vis, fluorimetric and CD data, Figures S20–S31, Table S2), Details of synthetic procedures and characterization of new peptidoids and precursors (NMR data: Figures S32–S47).

Author Contributions: M.K. and I.K. share the first authorship for equal contributions; synthesis and characterization of new compounds M.K., I.K. and B.Ž.; the study of interactions with biomacromolecules, M.K. and I.K.; supervision, conceptualization, funding acquisition, writing of the manuscript, B.Ž. and I.P. All authors have read and agreed to the published version of the manuscript.

Funding: This research was funded by the Croatian Science Foundation project IP-2018-01-5475.

Institutional Review Board Statement: Not applicable.

Informed Consent Statement: Not applicable.

Data Availability Statement: The data presented in this study are available in Supplementary Materials.

Acknowledgments: The authors are grateful to Nikola Basarić, Ruđer Bošković Institute, Zagreb, for the help in TC-SPC experiments and to Željka Ban, Ruđer Bošković Institute, Zagreb, for the help in synthetic experiments.

Conflicts of Interest: The authors declare no conflict of interest.

References

1. Rodzik, A.; Pomastowski, P.; Sagandykova, G.N.; Buszewski, B. Interactions of Whey Proteins with Metal Ions. *Int. J. Mol. Sci.* **2020**, *21*, 2156. [CrossRef] [PubMed]
2. Tisato, F.; Marzano, C.; Porchia, M.; Pellei, M.; Santini, C. Copper in diseases and treatments and copper-based anticancer strategies. *Med. Res. Rev.* **2010**, *30*, 708–749. [CrossRef]
3. Sathyadevi, P.; Krishnamoorthy, P.; Jayanthi, E.; Butorac, R.R.; Cowley, A.H.; Dharmaraj, N. Studies on the effect of metal ions of hydrazone complexes on interaction with nucleic acids, bovine serum albumin and antioxidant properties. *Inorg. Chim. Acta* **2012**, *384*, 83–96. [CrossRef]

4. Harding, M.M.; Nowicki, M.W.; Walkinshaw, M.D. Metals in protein structures: A review of their principal features. *Crystallogr. Rev.* **2010**, *16*, 247–302. [CrossRef]
5. Zou, J.; Sugimoto, N. Complexation of peptide with Cu^{2+} responsible to inducing and enhancing the formation of α-helix conformation. *BioMetals* **2000**, *13*, 349–359. [CrossRef] [PubMed]
6. Berg, J.M. *Metal Ions in Proteins: Structural and Functional Roles*; Cold Spring Harbor Laboratory Press: New York, NY, USA, 1987; Volume 52, pp. 579–585.
7. Horn, D.; Barrientos, A. Mitochondrial copper metabolism and delivery to cytochromec oxidase. *IUBMB Life* **2008**, *60*, 421–429. [CrossRef]
8. Katoh, S. Early research on the role of plastocyanin in photosynthesis. *Photosynth. Res.* **2003**, *76*, 255–261. [CrossRef]
9. Robinett, N.G.; Peterson, R.L.; Culotta, V.C. Eukaryotic copper-only superoxide dismutases (SODs): A new class of SOD enzymes and SOD-like protein domains. *J. Biol. Chem.* **2017**, *293*, 4636–4643. [CrossRef]
10. Solomon, E.I.; Heppner, D.E.; Johnston, E.M.; Ginsbach, J.W.; Cirera, J.; Qayyum, M.; Tian, L. Copper Active Sites in Biology. *Chem. Rev.* **2014**, *114*, 3659–3853. [CrossRef]
11. Laurie, S.H. *Handbook of Metal-Ligand Interactions in Biological Fluids: Bioinorganic Chemistry*; Berthon, G., Ed.; Marcel Dekker: New York, NY, USA, 1995; Volume 1, pp. 603–619.
12. Khoury, R.R.; Sutton, G.J.; Ebrahimi, D.; Hibbert, D.B. Formation constants of copper(II) complexes with tripeptides containing Glu, Gly, and His: Potentiometric measurements and modeling by generalized multiplicative analysis of variance. *Inorg. Chem.* **2014**, *53*, 1278–1287. [CrossRef]
13. Sóvágó, I.; Várnagy, K.; Lihi, N.; Grenács, Á. Coordinating properties of peptides containing histidyl residues. *Coord. Chem. Rev.* **2016**, *327–328*, 43–54. [CrossRef]
14. Rimola, A.; Rodríguez-Santiago, L.; Sodupe, M. Cation-pi Interactions and oxidative effects on Cu^{+} and Cu^{2+} binding to Phe, Tyr, Trp, and His amino acids in the gas phase. Insights from first-principles calculations. *J. Phys. Chem. B* **2006**, *110*, 24189–24199. [CrossRef]
15. Kozlowski, H.; Bal, W.; Dyba, M.; Kowalik-Jankowska, T. Specific structure-stability relations in metallopeptides. *Coord. Chem. Rev.* **1999**, *184*, 319–346. [CrossRef]
16. Crowley, J.D.; McMorran, D.A. Topics in Heterocyclic 100. *Chemistry* **2012**, *28*, 31.
17. Bedeche, S.; Daran, J.-C.; Ruiz, J.; Astruc, D. Synthesis and coordination chemistry of ferrocenyl-1, 2, 3-triazolyl ligands. *Inorg. Chem.* **2008**, *47*, 4903–4908. [CrossRef]
18. Valverde, I.E.; Mindt, T.L. 1,2,3-Triazoles as Amide-bond Surrogates in Peptidomimetics. *CHIMIA* **2013**, *67*, 262–266. [CrossRef]
19. Hamdan, F.; Tahoori, F.; Balalaie, S. Synthesis of novel cyclopeptides containing heterocyclic skeletons. *RSC Adv.* **2018**, *8*, 33893–33926. [CrossRef]
20. Bonnamour, J.; Legros, J.; Crousse, B.; Bonnet-Delpon, D. Synthesis of new trifluoromethyl peptidomimetics with a triazole moiety. *Tetrahedron Lett.* **2007**, *48*, 8360–8362. [CrossRef]
21. Agalave, S.G.; Maujan, S.R.; Pore, V.S. Click Chemistry: 1,2,3-Triazoles as Pharmacophores. *Chem. Asian J.* **2011**, *6*, 2696–2718. [CrossRef]
22. Kharb, R.; Sharma, P.C.; Yar, M.S. Pharmacological significance of triazole scaffold. *J. Enzym. Inhib. Med. Chem.* **2010**, *26*, 1–21. [CrossRef]
23. Sivakumar, K.; Xie, F.; Cash, B.M.; Long, S.; Barnhill, H.N.; Wang, Q. A Fluorogenic 1,3-Dipolar Cycloaddition Reaction of 3-Azidocoumarins and Acetylenes. *Org. Lett.* **2004**, *6*, 4603–4606. [CrossRef] [PubMed]
24. Mama, N.; Battison, A. Synthesis and application of a fluorescent "turn-off" triazolyl-coumarin-based fluorescent chemosensor for the sensing of Fe^{3+} ions in aqueous solutions. *Arkivoc* **2020**, *5*, 59–84. [CrossRef]
25. Singh, G.; Satija, P.; Singh, A.; Diksha, A.; Pawan, A.; Suman, A.; Sushma, A.; Mohit, A.; Soni, S. Azo dye featuring triazole appended organosilicon multifunctionalized sensor: Paradigm for detection of Cu^{+2} and Fe^{+2} ions. *Mater. Chem. Phys.* **2020**, *249*, 123005. [CrossRef]
26. Musa, M.A.; Cooperwood, J.S.; Khan, M.O.F. A review of coumarin derivatives in pharmacotherapy of breast cancer. *Curr. Med. Chem.* **2008**, *15*, 2664–2679. [CrossRef]
27. Canning, C.; Sun, S.; Ji, X.; Gupta, S.; Zhou, K. Antibacterial and cytotoxic activity of isoprenylated coumarin mammea A/AA isolated from Mammea Africana. *J. Ethnopharmacol.* **2013**, *147*, 259–262. [CrossRef]
28. Nizamov, S.; Willig, K.I.; Sednev, M.V.; Belov, V.N.; Hell, S.W. Phosphorylated 3-Heteroarylcoumarins and Their Use in Fluorescence Microscopy and Nanoscopy. *Chem. Eur. J.* **2012**, *18*, 16339–16348. [CrossRef] [PubMed]
29. Wang, C.; Lu, L.; Ye, W.; Zheng, O.; Qiu, B.; Lin, Z.; Guo, L.; Chen, G. Fluorescence sensor for Cu(II) in the serum sample based on click chemistry. *Analyst* **2014**, *139*, 656–659. [CrossRef]
30. Mital, M.; Wezynfeld, N.E.; Frączyk, T.; Wiloch, M.Z.; Wawrzyniak, U.E.; Bonna, A.; Tumpach, C.; Barnham, K.J.; Haigh, C.L.; Bal, W.; et al. A functional role for Aβ in metal homeostasis? N-truncation and high-affinity copper binding. *Angew. Chem.* **2015**, *127*, 10606–10610. [CrossRef]
31. Mital, M.; Szutkowski, K.; Bossak-Ahmad, K.; Skrobecki, P.; Drew, S.C.; Poznański, J.; Zhukov, I.; Frączyk, T.; Bal, W. The Palladium(II) Complex of Aβ4−16 as Suitable Model for Structural Studies of Biorelevant Copper(II) Complexes of N-Truncated Beta-Amyloids. *Int. J. Mol. Sci.* **2020**, *21*, 9200. [CrossRef]

32. Gonzalez, P.; Bossak, K.; Stefaniak, E.; Hureau, C.; Raibaut, L.; Bal, W.; Faller, P. N-Terminal Cu-Binding Motifs (Xxx-Zzz-His, Xxx-His) and Their Derivatives: Chemistry, Biology and Medicinal Applications. *Chem.-Eur. J.* **2018**, *24*, 8029–8041. [CrossRef]
33. Li, L.B.; Vorobyov, I.; Allen, T.W. The Different Interactions of Lysine and Arginine Side Chains with Lipid Membranes. *J. Phys. Chem. B* **2013**, *117*, 11906–11920. [CrossRef]
34. Mergny, J.L.; Lacroix, L. Analysis of Thermal Melting Curves. *Oligonucleotides* **2003**, *13*, 515–537. [CrossRef]
35. Feldman, A.K.; Colasson, B.; Fokin, V.V. One-Pot Synthesis of 1,4-Disubstituted 1,2,3-Triazoles from In Situ Generated Azides. *Org. Lett.* **2004**, *6*, 3897–3899. [CrossRef]
36. Hassan, S.; Müller, T.J.J. Multicomponent syntheses based upon copper-catalyzed alkyne-azide cycloaddition. *Adv. Synth. Catal.* **2015**, *357*, 617–666. [CrossRef]
37. Aioub, A.G.; Dahora, L.; Gamble, K.; Finn, M.G. Selection of Natural Peptide Ligands for Copper-Catalyzed Azide–Alkyne Cycloaddition Catalysis. *Bioconjug. Chem.* **2017**, *28*, 1693–1701. [CrossRef] [PubMed]
38. Hoshiyama, M.; Kubo, K.; Igarashi, T.; Sakurai, T. Complexation and proton dissociation behavior of 7-hydroxy-4-methylcoumarin and related compounds in the presence of beta-cyclodextrin. *J. Photochem. Photobiol. A Chem.* **2001**, *138*, 227–233. [CrossRef]
39. Gampp, H.; Maeder, M.; Meyer, C.J.; Zuberbuhler, A.D. Calculation of Equilibrium-Constants from Multiwavelength Spectroscopic Data.2. Specfit-2 User-Friendly Programs in Basic and Standard Fortran-77. *Talanta* **1985**, *32*, 257–264. [CrossRef]
40. Maeder, M.; Zuberbuehler, A.D. Nonlinear Least-Squares Fitting of Multivariate Absorption Data. *Anal. Chem.* **1990**, *62*, 2220–2224. [CrossRef]
41. Alies, B.; Renaglia, E.; Rozga, M.; Bal, W.; Faller, P.; Hureau, C. Cu(II) Affinity for the Alzheimer's Peptide: Tyrosine Fluorescence Studies Revisited. *Anal. Chem.* **2013**, *85*, 1501–1508. [CrossRef] [PubMed]
42. Pescitelli, G.; Di Bari, L.; Berova, N. Conformational aspects in the studies of organic compounds by electronic circular dichroism. *Chem. Soc. Rev.* **2011**, *40*, 4603–4625. [CrossRef]
43. Saha, B.; Ikbal, S.A.; Petrovic, A.G.; Berova, N.; Rath, S.P. Complexation of Chiral Zinc-Porphyrin Tweezer with Achiral Diamines: Induction and Two-Step Inversion of Interporphyrin Helicity Monitored by ECD. *Inorg. Chem.* **2017**, *56*, 3849–3860. [CrossRef] [PubMed]
44. Chen, Y.; Petrovic, A.G.; Roje, M.; Pescitelli, G.; Kayser, M.M.; Yang, Y.; Berova, N.; Proni, G. CD-Sensitive Zn-Porphyrin Tweezer Host-Guest Complexes, Part 2: Cis- and Trans-3-Hydroxy-4-aryl/alkyl-beta-Lactams. A Case Study. *Chirality* **2010**, *22*, 140–152. [CrossRef] [PubMed]
45. McGhee, J.D.; von Hippel, P.H. Theoretical aspects of DNA-protein interactions: Co-operative and non-co-operative binding of large ligands to a one-dimensional homogeneous lattice. *J. Mol. Biol.* **1974**, *86*, 469–489. [CrossRef]
46. Sedgwick, A.C.; Brewster, J.T.; Wu, T.H.; Feng, X.; Bull, S.D.; Qian, X.H.; Sessler, J.L.; James, T.D.; Anslyn, E.V.; Sun, X.L. Indicator displacement assays (IDAs): The past, present and future. *Chem. Soc. Rev.* **2021**, *50*, 9–38. [CrossRef] [PubMed]
47. Eriksson, M.; Norden, B. Linear and Circular Dichroism of Drug-Nucleic Acid Complexes. *Methods Enzymol.* **2001**, *340*, 68–98. [PubMed]
48. Šmidlehner, T.; Piantanida, I.; Pescitelli, G. Polarization Spectroscopy Methods in the Determination of Interactions of Small Molecules with Nucleic Acids-Tutorial. *Beilstein J. Org. Chem.* **2018**, *14*, 84–105. [CrossRef]